



Bioreduction of nitrate in high-sulfate water using a hydrogen-based membrane biofilm reactor equipped with a separate carbon dioxide module

Siqing Xia^{a,b,*}, Chengyang Wu^{a,b}, Xiaoxiao Yang^{a,b}, Yun Zhou^c, Luman Zhou^{a,b}, Yajun Ran^{a,b}, Bruce E. Rittmann^d

^a State Key Laboratory of Pollution Control and Resource Reuse, College of Environmental Science and Engineering, Tongji University, Shanghai 200092, China

^b Shanghai Institute of Pollution Control and Ecological Security, Shanghai 200092, China

^c University of Alberta, Department of Civil and Environmental Engineering, Edmonton, Alberta T6G 1H9, Canada

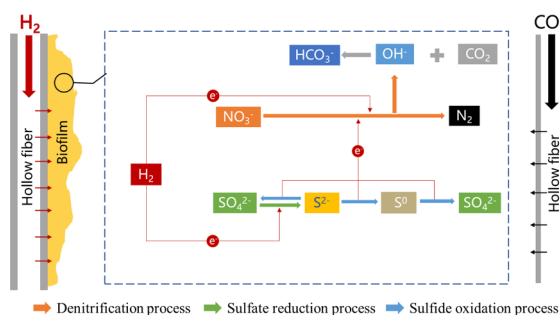
^d Biodesign Swette Center for Environmental Biotechnology, Arizona State University, USA



HIGHLIGHTS

- pH value at 7~8 was maintained by CO₂ membranes in long term operation.
- Net SO₄²⁻ reduction was controlled by NO₃⁻ loading in MBfR due to sulfide oxidation.
- Sulfide oxidation provided extra electron flow pathways to denitrification.
- Sulfate-reducing bacteria and sulfide-oxidizing bacteria drove closed S-cycling.

GRAPHICAL ABSTRACT



ARTICLE INFO

Keywords:

Membrane biofilm reactor
 Hydrogen (H₂)
 Denitrification
 Sulfate reduction
 Sulfide oxidation

ABSTRACT

A hydrogen-based membrane biofilm reactor (MBfR) equipped with separate hydrogen (H₂) and carbon dioxide (CO₂) adjustable gas-transfer modules was used to explore denitrification in a water containing a high concentration of sulfate (SO₄²⁻) (500 mg S/L). CO₂ was used for pH control and as the sole carbon source for long-term operation of the MBfR, during which > 90% denitrification was achieved. Short-term experiments demonstrated that increasing the SO₄²⁻ loading had negligible effect on nitrate (NO₃⁻) reduction, but SO₄²⁻ reduction was strongly suppressed by high NO₃⁻ loading regardless of H₂ availability. Sulfide oxidation accompanied with SO₄²⁻ reduction occurred in the biofilm, and the intermediate element sulfur was further oxidized to SO₄²⁻. Results of high-throughput sequencing suggest that sulfide oxidation was carried out by the known sulfide-oxidizing bacteria: *Starkeya* and *Xanthobacter*. And sulfide oxidation coupled to denitrification was a primary reason for minimal net SO₄²⁻ reduction when the NO₃⁻ loading was high enough. This study demonstrates the promise of effective denitrification without net SO₄²⁻ reduction in MBfR systems and documents the important sulfur-conversion processes.

* Corresponding author at: State Key Laboratory of Pollution Control and Resource Reuse, College of Environmental Science and Engineering, Tongji University, Shanghai 200092, China.

E-mail address: siqingxia@gmail.com (S. Xia).

<https://doi.org/10.1016/j.cej.2019.123831>

Received 8 October 2019; Received in revised form 29 November 2019; Accepted 14 December 2019

Available online 16 December 2019

1385-8947/ © 2019 Elsevier B.V. All rights reserved.

1. Introduction

NO_3^- and NO_2^- are electron acceptors commonly found in agricultural runoff, groundwater, and industrial and municipal wastewaters. The U.S. EPA set maximum contaminant levels (MCLs) of 10 mg N/L for NO_3^- and 1 mg N/L for NO_2^- [1] due to their health risk [2]. Denitrification by hydrogenotrophic autotrophic biofilms is a promising means to remove nitrate and nitrite [3–6], these denitrifying bacteria (DB) are found throughout the *Proteobacteria*, and well-established genera include *Dechloromonas* (β -proteobacteria), *Hydrogenophaga* (β -proteobacteria), and *Xanthobacter* (α -proteobacteria) [7–10].

Sulfate (SO_4^{2-}) is an electron acceptor that is frequently found in water and wastewater. Dissimilatory SO_4^{2-} reduction, the sulfate-reducing bacteria (SRB) reduce SO_4^{2-} to form sulfide, is driven by series of enzymes: with consumption of one molecule of ATP, SO_4^{2-} was activated by an ATP sulfurylase producing adenosine phosphosulfate (APS) and pyrophosphate. After the activation, an APS reductase reduces APS to sulfite (SO_3^{2-}) and adenosine monophosphate (AMP), and a sulfite reductase converts SO_3^{2-} to sulfide [5,11]. Minimizing SO_4^{2-} reduction is normally an important objective when SO_4^{2-} and NO_3^- are present in the same water [6,8,12,13], since sulfide, the SO_4^{2-} -reduction product, can inhibit denitrification [14] and create an extra H_2 demand.

The hydrogen-based membrane biofilm reactor (MBfR) that delivers hydrogen gas (H_2) to a biofilm by diffusion through the walls of bubbleless gas-transfer membranes has been used to achieve denitrification in the presence of SO_4^{2-} . Researches have conducted to investigate reduction of SO_4^{2-} in a denitrifying MBfR fed with a moderate SO_4^{2-} concentration (< 100 mg SO_4^{2-} /L) [8,12,15,16]. These studies concluded that SO_4^{2-} reduction occurred when NO_3^- was almost completely removed, but was insignificant when the H_2 -delivery capacity was only enough to accomplish denitrification. Thus, SO_4^{2-} reduction could be suppressed by carefully limiting the delivery capacity of H_2 .

Denitrification can be made more challenging when the water contains a high concentration of SO_4^{2-} , such as ≥ 1000 mg SO_4^{2-} /L. High-sulfate wastewaters occur in the rubber industry [17], oil-production wastewater [18], mine drainage [19], and flue-gas desulfurization [20]. High SO_4^{2-} loading might stimulate the growth of SRB that compete with denitrifiers for H_2 as the electron donor. However, the competition advantages of denitrification over SO_4^{2-} reductions in a hydrogen-based biofilm may alter in a water containing high-sulfate, which has not been studied.

A promising approach to minimize net sulfate reduction is to allow

sulfide oxidation through autotrophic denitrification using sulfide as an electron donor [21,22]. SO_4^{2-} reduced to sulfide by SRB is re-oxidized by sulfide-oxidizing bacteria (SOB). Full sulfide oxidation, back to SO_4^{2-} , leads to no net SO_4^{2-} reduction, but partial sulfide oxidation also is possible. No net SO_4^{2-} reduction is an ideal outcome, because it eliminates the troublesome aspect of SO_4^{2-} reduction and creates no additional demand for H_2 beyond that of denitrification. End-product distribution of sulfide oxidation depends on the sulfide to nitrate (S/N) ratio [23,24], and an S/N ratio < 0.5 mol/mol fostered almost complete re-oxidation to SO_4^{2-} . A greater S/N ratio led to accumulation of sulfide and partial oxidation in expense of sulfide oxidation to elemental sulfur (S^0) that led to net sulfate reduction and proportionally increased demand for H_2 .

pH control is another practical challenge, since reduction of oxyanions consumes protons and increases the pH [5,25,26], which can lead to inhibition of metabolic activity and mineral precipitates [25,27,28]. Bubbleless CO_2 delivered by hollow-fiber membranes [29,30] is a simple option for pH control in a H_2 -based MBfR, particularly since it also provides the inorganic carbon source for the autotrophs. The demand for CO_2 to neutralize alkali is the driving force to pull CO_2 through the membrane, and CO_2 -delivery capacity can be controlled by CO_2 pressure [31,32]. Thus, membrane delivery of CO_2 can bring about pH stability and inorganic-C delivery in one simple step.

In this study, we evaluated the denitrification capability of a bench-scale MBfR with separate membranes for delivering H_2 and CO_2 when the influent water contained a high concentration of SO_4^{2-} . The overarching objective was to develop a management strategy to achieve full NO_3^- reduction while suppressing SO_4^{2-} reduction and document the mechanisms underlying SO_4^{2-} reduction and oxidation. Specific objectives were (1) to determine how manipulating the H_2 pressure and NO_3^- loading could counteract a high SO_4^{2-} loading and allow NO_3^- reduction without net SO_4^{2-} reduction; (2) to define the role of sulfide oxidation in suppressing net sulfate reduction; and (3) to understand how the structure and function of the microbial community was related to success or failure of the first specific objective.

2. Materials and methods

2.1. MBfR setup

The MBfR setup used in this study (shown in Fig. 1), modified from our previous nitrate-bioreduction study [31], consisted of a transparent plastic cylinder sealed with a plastic ring, silicone pipelines, and peristaltic pumps (Lange BT100-2J, China). The reactor was 25 cm in

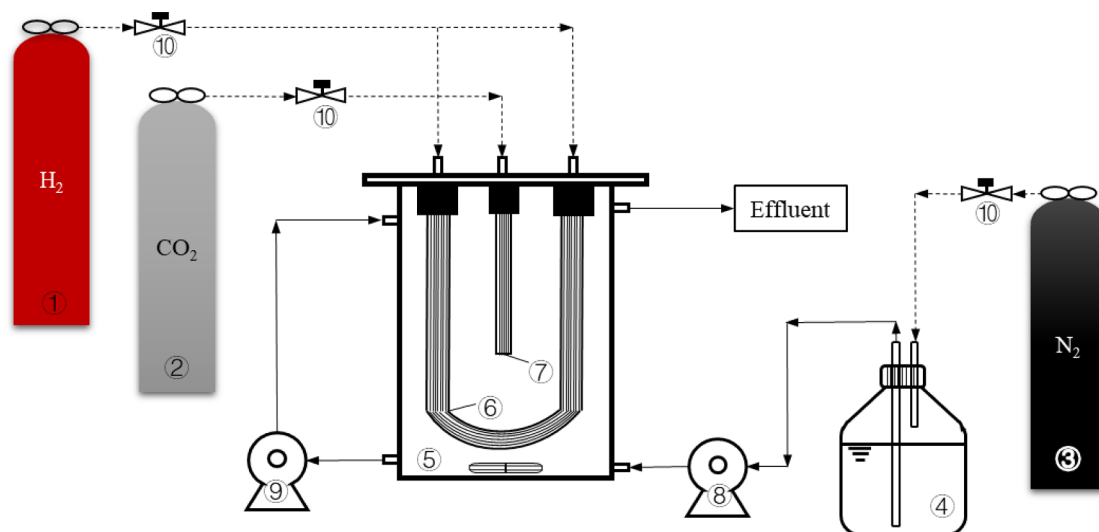


Fig. 1. Schematic of the MBfR system.

height and 8 cm in inner diameter. All membranes used in the reactor were polyvinyl chloride (PVC) hollow fibers with an outer diameter of 0.18 cm, an inner diameter of 0.12 cm, and average pore size of 0.1 μm (Litree Company, Suzhou, China). The reactor contained one main bundle (65 fibers) that was 36 cm long. Both ends of the main bundle were connected to the pure H_2 gas-delivery pipeline. A supplementary bundle of 30 fibers (15-cm long) was pressurized with pure CO_2 . The total surface area of H_2 and CO_2 -delivering membranes were 882 and 254 cm^2 , respectively. The reactor had a 630-mL working volume and the liquid was mixed by a magnetic stirring bar at the bottom of the reactor and by a peristaltic pump giving a recirculation rate of 150 mL/min. In all experiments, the medium was stored in a 10-L glass bottle purged with N_2 to eliminate the dissolved oxygen (DO) lower than 0.2 mg/L. The temperature was controlled at 25 ± 1 $^\circ\text{C}$.

2.2. Enriching denitrifying microorganisms

Activated sludge collected from an anoxic tank in the Quyang wastewater treatment plant (Yangpu, Shanghai) was used to inoculate the MBfR. The enrichment medium contained the following compounds (mg/L): $\text{CaCl}_2 \cdot 2\text{H}_2\text{O}$ 1; FeCl_2 1; MgCl_2 10; ZnCl_2 0.013; H_3BO_3 0.038; $\text{CuCl}_2 \cdot 2\text{H}_2\text{O}$ 0.001; $\text{MoO}_4 \cdot 2\text{H}_2\text{O}$ 0.004; $\text{MnCl}_2 \cdot 4\text{H}_2\text{O}$ 0.004; $\text{CoCl}_2 \cdot 6\text{H}_2\text{O}$ 0.025; $\text{NiCl}_2 \cdot 6\text{H}_2\text{O}$ 0.001; and Na_2SeO_3 0.003. NaHCO_3 and NaNO_3 were added as carbon and nitrogen sources for the growth of autotrophic microorganisms, respectively. A 5-mM phosphate buffer (Na_2HPO_4 and KH_2PO_4) was added into the feed water to stabilize its pH at 7.1 ± 0.1 . Enrichment was carried out in 250-mL glass-bottle with 100 mL H_2 in the headspace. NaNO_3 was added as the sole electron acceptor and NaHCO_3 as the sole carbon source. After 2 days, the NO_3^- concentration decreased below the detection limit, and NO_3^- was replenished. After another 2 days, an acclimated autohydrogenotrophic denitrifying inoculum was used to inoculate for the MBfR.

2.3. Reactor startup and continuous operation

The MBfR was inoculated with 50 mL of suspended biomass from the enrichment culture. The composition of the feed medium to the MBfR was the same as the enrichment medium, except as noted for each stage and substage, as summarized in Table 1. Once CO_2 was supplied via the membranes, NaHCO_3 was reduced gradually and replaced by CO_2 , and the phosphate buffer was removed during continuous

operation. The maximum CO_2 -delivery capacity at 1.8 atm was 3.24 $\text{g}/\text{m}^2\text{-d}$, calculated according to Xia et al. [31].

2.4. Short-term experiments

Before the start of short-term experiments, the MBfR was fed continuously with SO_4^{2-} -containing influent so that the biofilm of MBfR could acclimate to SO_4^{2-} (stage 2). After SO_4^{2-} exposure for 35 days, the effluent concentrations of all N and S species were stable ($< 10\%$ deviation over three days), and a series of short-term experiments was used to investigate the effect of SO_4^{2-} loadings, H_2 pressure, and NO_3^- loadings on NO_3^- and SO_4^{2-} reductions. The experiments were organized into three series, as noting in Table 1. Prior to each short-term test, the reactor was returned to the baseline condition, which was a simulated wastewater having 30 mg N/L of NO_3^- , 500 mg S/L of SO_4^{2-} (~ 1400 mg $\text{SO}_4^{2-}/\text{L}$), 1.6 atm for H_2 , and 1.8 atm for CO_2 ; baseline loading lasted until the concentration of all N and S species in the effluent became stable. Each substage lasted 52.5 h, equivalent to 5 HRTs, long enough for the system to reach a steady state for the liquid phase [33]. Replicate samples were collected at 3, 4, and 5 HRTs, and the results are reported as the average values \pm the standard deviation.

2.5. Practical wastewater experiments

After the conclusion of the short-term experiments, we replaced the synthetic wastewater by actual wastewater composed of 85% (by volume) domestic sewage plus 15% dyeing effluent from the Quyang wastewater treatment plant (Shanghai, China). The actual wastewater was fed to the MBfR continually for 80 days, but we changed the HRT in a series of three substages (Table 1). When the concentration of all N and S species in effluent stabilized, we calculated the contaminants removal and flux.

2.6. Sampling and analytical methods

MBfR influent and effluent samples were collected routinely and immediately filtered through a 0.22- μm membrane filter (Anpel Company, Shanghai, China). NO_3^- , NO_2^- , SO_3^{2-} , and SO_4^{2-} were measured by ion chromatography (ICS-1000, Dionex, USA) using an AS-19 column. NH_4^+ was measured using Nessler's reagent colorimetric method according to Standard Methods (GB 7479-87, China). The

Table 1

Operational parameters for all stages and substages.

Stages	Substages	Water	Influent NO_3^- -N (mg/L)	Influent SO_4^{2-} (mg S/L)	Influent HCO_3^- (mg/L)	H_2 pressure (atm)	CO_2 pressure (atm)	HRT (h)	Duration (d)
1	1	Synthetic wastewater	30	0	80	1.6	0	10.5	30
	2		30	0	80		1.8		10
	3		30	0	40		1.8		10
	4		30	0	0		1.8		10
2			30	500	0	1.6	1.8	10.5	35
	3						1.8	10.5	75
3	A1		30	10	0	1.6			
	A2		30	35	0	1.6			
	A3		30	100	0	1.6			
	A4		30	250	0	1.6			
	A5		30	500	0	1.6			
	B1		30	500	0	1.2			
	B2		30	500	0	1.4			
	B3		30	500	0	1.6			
	B4		30	500	0	1.8			
	C1		0	500	0	1.6			
	C2		10	500	0	1.6			
	C3		20	500	0	1.6			
	C4		30	500	0	1.6			
	C5		40	500	0	1.6			
	4	1	Actual wastewater	33	470	0	1.6	1.8	31.5
2				470	0			10.5	27
3				470	0			5.2	26

dissolved sulfide concentration was analyzed using a colorimetric method based on methylene blue formation [34]. Considering all the possible products of SO_4^{2-} reduction (i.e., SO_3^{2-} , S^0 , and sulfide), the concentration of S^0 (mg S/L) was calculated based on sulfur mass balance: (S^0 -S removal = Inf. SO_4^{2-} -S - Eff. SO_4^{2-} -S - Eff. SO_3^{2-} -S - Eff. sulfide-S) [23]. We also measured the pH of unfiltered influent and effluent samples at least three times daily using a pH meter (HQ40d, HACH, USA).

The solids collected from biofilm were washed by deoxygenated water, freeze dried, and characterized using X-ray diffraction (Bruker D8 advance XRD, Germany) using Cu-K α radiation and Organic chemical elemental analyzer (CHON, Elementar Vario EL III, German) to analyze S^0 concentration in biofilm solid.

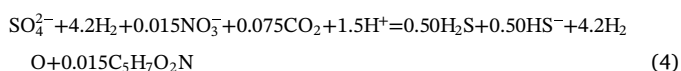
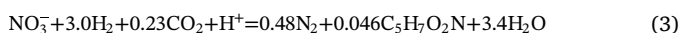
2.7. Electron-equivalent fluxes analysis

The surface loadings (J^{max}) and removal fluxes (J) of an electron-acceptor substrate ($\text{g}/\text{m}^2\text{-d}$) were calculated with Eqs. (1) and (2), respectively [35]:

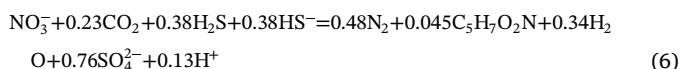
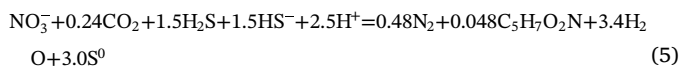
$$J^{\text{max}} = \frac{QS_0}{A} \quad (1)$$

$$J = \frac{Q(S_0 - S)}{A} \quad (2)$$

where Q is the influent flow rate, m^3/d ; S_0 and S refer to the influent concentration and effluent concentration of the substrate (SO_4^{2-} and NO_3^-), respectively, g/m^3 ; A is the surface area of the membrane, m^2 . Electron-consumption flux was computed from the removal fluxes and reaction stoichiometry shown in Eq. (3) for denitrification and sulfate reduction to sulfide in Eq. (4) when using H_2 as the sole electron donor:



Considering that sulfide is an electron donor, NO_3^- flux was divided into 3 parts: NO_3^- flux 1 represents electron-equivalents transferred to NO_3^- from sulfide for its partial oxidation to S^0 (Eq. (5)); NO_3^- flux 2 represents electron-equivalents transferred to NO_3^- from sulfide for its complete oxidation to SO_4^{2-} (Eq. (6)); NO_3^- flux 3 represents electron-equivalents transferred to NO_3^- from H_2 (Eq. (3)); the net SO_4^{2-} flux represents electron equivalents retained in sulfide and S^0 and was computed by subtracting the electron-equivalents for sulfide oxidation to S^0 from the measured SO_4^{2-} flux (Eq. (4)), which means net electron equivalent flows to SO_4^{2-} (i.e., net SO_4^{2-} flux = measured SO_4^{2-} flux - NO_3^- flux 1).



The H_2 flux in $\text{g H}_2/\text{m}^2\text{-d}$ has the same value as the H_2 flux in $\text{e}^- \text{eq}/\text{m}^2\text{-d}$, and a sulfide flux of $1 \text{ g S}/\text{m}^2\text{-d}$ is equal to $0.1875 \text{ e}^- \text{eq}/\text{m}^2\text{-d}$. All reactions include biomass ($\text{C}_5\text{H}_7\text{O}_2\text{N}$) net synthesis.

We also calculated the unused H_2 flux from the measured effluent H_2 concentration (S):

$$J_{\text{H}_2} = \frac{QS}{A} \quad (7)$$

Finally, the maximum delivery fluxes of H_2 and CO_2 were determined by the methods of Tang et al. [36] and Xia et al. [31].

2.8. Microbial community analysis

We collected the inoculation sludge and biofilms at the end of stages 1 and 2. Biofilm samples were pieces of membrane cut from the fiber bundler using an autoclaved scissors. We followed the procedures of biofilm separation and DNA extraction described by Xia et al. [30]. In brief, NGS library preparations and Illumina MiSeq sequencing were conducted at GENEWIZ, Inc. (Beijing, China). DNA samples were quantified using a Qubit 2.0 Fluorometer (Invitrogen, Carlsbad, CA, USA), and DNA quality was checked on a 0.8% agarose gel. We performed amplicon sequencing of the V3 and V4 region of the 16S rRNA genes using the barcoded primer set 338F (5'-ACTCCTACGGGAGGCA GCA-3') and 806R (5'-GGACTACHVGGGTWTCTAAT-3'), and sequence results were processed and analyzed on QIIME platform [37]; the detailed protocol was described by Long et al. [7]. We picked the operational taxonomic unit (OTUs) using the Greengenes database with uclust based on $\geq 97\%$ identity, randomly picking 5500 sequences per sample and removed OTUs contain fewer than 2 sequences from our analysis and aligned representative sequences of OTUs to the Greengenes Database using PyNast. To assign taxonomy to OTUs, we assigned taxonomy to the OTUs using the Greengenes database using confidence threshold of 0.8. Primers also contain adaptor sequences that allow uniform amplification of the library with high complexity ready for downstream NGS sequencing on Illumina Miseq, the 16S rRNA genes target-specific sequence.

3. Results and discussion

3.1. Denitrification using CO_2 as carbon source and pH buffer

Stage 1 was used to document that CO_2 could be the sole carbon source and the sole pH buffer in the denitrifying MBfR. In its role as a pH buffer, CO_2 counteracted base formation from oxyanion reduction. The pH dropped to 6.0 at first (Fig. S1 in Supplementary Information), but recovered to 7.3 in two days, once denitrification became established and generated base. On day 50, we removed bicarbonate from the influent to verify that CO_2 could be the sole carbon source for the biofilm. The maximum CO_2 delivery capacity ($3.2 \text{ g}/\text{m}^2\text{-d}$) exceeded the CO_2 consumption needed for OH^- neutralization and being the carbon source ($1.9 \text{ g}/\text{m}^2\text{-d}$, calculated by Eq. (3)). At the end of stage 1, 100% denitrification was achieved (the NO_3^- flux was $0.22 \text{ e}^- \text{eq}/\text{m}^2\text{-d}$), and the pH was stable at 7.9 ± 0.1 , verifying the applicability of membrane delivery of CO_2 for long-term operation.

3.2. Effects of relative availabilities of H_2 and the electron acceptors

Series of short-term tests evaluated the effects of changing the relative availabilities of H_2 (the electron donor) and SO_4^{2-} or NO_3^- (the electron acceptors) on denitrification and SO_4^{2-} reduction. The availabilities were directly compared according to their electron-equivalent loadings or fluxes ($\text{e}^- \text{eq}/\text{m}^2\text{-d}$). The effects were evaluated in three series: Increasing SO_4^{2-} loading, increasing H_2 delivery capacity, and increasing NO_3^- loading (the A, B, and C series, respectively, in Table 1).

3.2.1. NO_3^- reduction is not affected by higher SO_4^{2-} loading

The first short-term experiments began after 35 days of acclimation to influent SO_4^{2-} (shown in Fig. S2, S3); effluent SO_4^{2-} concentration was stable and previous studies showed that 35 days was long enough to establish sulfate reduction in the MBfR [12,33,38]. The effluent concentrations of NO_3^- -N, SO_4^{2-} , and sulfide are shown in Fig. 2a. NO_2^- was not detected in A substages, while SO_3^{2-} and NH_4^+ were not detected in all experiments. The sum of effluent SO_4^{2-} -S and sulfide concentrations was almost equal to influent SO_4^{2-} -S concentration, which shows good mass-balance closure for S and that S^0 accumulation was minimal. The effluent H_2 concentration was stable at $\sim 370 \mu\text{g}/\text{L}$

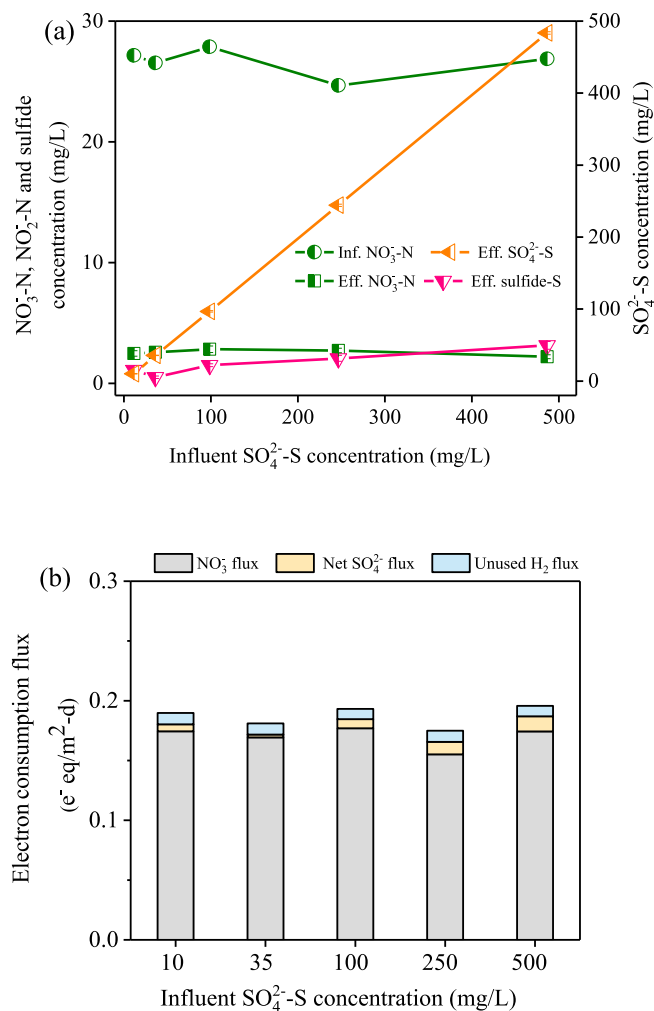


Fig. 2. Results for the A substages, in which the SO₄²⁻ loading was increased.

for all these conditions (Fig. S3a, in SI), much higher than the half-maximum-rate concentration for H₂ in SO₄²⁻ reduction (22 μg H₂/L [39]), indicating that H₂ availability was not a limiting factor for SO₄²⁻ reduction.

NO₃⁻ removal was stable at ~93% in these substages, and Fig. 2b shows that the electron equivalent fluxes of NO₃⁻ removal and effluent H₂ (noted as the unused H₂ flux) also were stable at ~0.17 and ~0.01 e⁻ eq/m²-d, respectively. Although the net SO₄²⁻ flux rose a small amount with higher SO₄²⁻ loading (up to a flux of 0.013 e⁻ eq/m²-d for the surface loading of 2.1 e⁻ eq/m²-d), SO₄²⁻ reduction was minor, no more than 1% of influent SO₄²⁻. Thus, an increased influent SO₄²⁻ concentration scarcely promoted SO₄²⁻ reduction, and NO₃⁻ reduction remained unaffected. The likely reason is that denitrifiers dominated the competition between DB and SRB for space in the biofilm (discussed below, Section 3.4), which led to low SRB abundance in the biofilm.

Modeling [40] described how SRB can compete well for space in the biofilm only when their specific growth rate approaches the specific growth rate of inherently faster-growing DB. The highest nitrate concentration to allow more SO₄²⁻ reduction was 0.12 mg N/L if the SO₄²⁻ concentration was 483 mg S/L, and the H₂ was 370 μg/L in the liquid (effluent). In the A substages, the effluent NO₃⁻ concentration was ~2.5 mg N/L, which is consistent with DB having a competitive advantage for space at outside surface of the biofilm (the growth rates of DB and SRB calculated from effluent NO₃⁻ and SO₄²⁻ concentration were ~0.61 and ~0.21 d⁻¹, respectively). SO₄²⁻ reduction was small and not sensitive to the influent SO₄²⁻ concentration, since the SO₄²⁻ concentration in the biofilm was typically higher than half-maximum-

rate concentration of SO₄²⁻ (0.16–31 mg SO₄²⁻/L [5]) due to the reasons that sulfate is bioavailable, and minor net sulfate reduction happened. These modeling results account for the reason why increasing the SO₄²⁻ loading had negligible effect on NO₃⁻ reduction at a moderate NO₃⁻ loading.

3.2.2. Higher H₂ availability promoted NO₃⁻ reduction more than SO₄²⁻ reduction

The H₂-delivery capacity, set by the H₂ pressure, provides an upper limit on the removal flux of electron-acceptor substrates [36]. In the B substages, the H₂ pressure was increased stepwise from 1.2 to 1.8 atm (absolute pressure), and the concentrations of the compounds are shown in Fig. 3a. Mass balance closure for S was achieved, with almost 100% of the reduced SO₄²⁻ recovered as sulfide, which means that S⁰ did not accumulate in the biofilm. NO₃⁻ reduction was strongly controlled by H₂ pressure. The lowest H₂ pressure (1.2 atm) did not have enough H₂-delivery capacity (0.18 e⁻ eq/m²-d) to support complete denitrification. NO₃⁻ removal was only ~74% at 1.2 atm, NO₂⁻ accumulated in the effluent (2.1 ± 0.2 mg N/L), and the effluent H₂ concentration was zero (Fig. S3b in SI), leading to an unused-H₂ flux of zero (Fig. 3b).

Once the H₂ pressure was increased to 1.6 atm, NO₃⁻ removal was 93%, NO₂⁻ was not detected, and H₂ appeared in the effluent, giving a flux of unused H₂. Whereas, the higher H₂ pressure only slightly increased SO₄²⁻ reduction, which suggests that H₂ competition between SO₄²⁻ and NO₃⁻ was not the major reason why SO₄²⁻ reduction was repressed. The further increase of H₂ pressure to 1.8 atm, SO₄²⁻ reduction constituted only 10% of H₂ consumption, compared to 84% for denitrification, although the H₂ concentration in the effluent rose to ~600 μg/L, a value much higher than a typical half-saturation concentration for H₂ in SO₄²⁻ reduction [5], and the unused-H₂ flux increased to 7% of the total electron-equivalent flux.

3.2.3. Increased NO₃⁻ loading suppressed SO₄²⁻ reduction

To verify and more deeply evaluate the inhibitory effect of denitrification on net SO₄²⁻ reduction, the influent NO₃⁻-N concentration was increased stepwise from 0 to 40 mg/L in the C substages. We assumed that the abundance of SRB that drove SO₄²⁻ reduction in the biofilm was stable, because the reactor was operated in a pseudo-steady state condition [33]. Thus, we interpret that a lower net SO₄²⁻ flux at a higher NO₃⁻ loading was due to sulfide oxidation coupled to denitrification. We calculated the electron-equivalent fluxes based on the stoichiometry for the combinations of electron donors and different sulfide oxidation products in Eqs. (3)–(6), and these results are exhibited in Fig. 4b.

Fig. 4 summarizes the results for concentrations and electron-equivalent fluxes for the C substages. The effluent sulfide was 31.8 mg/L when influent NO₃⁻ was absent and decreased with higher influent NO₃⁻ concentration. The maximum net SO₄²⁻ flux (0.14 ± 0.03 e⁻ eq/m²-d) occurred in substage C1, when influent NO₃⁻ was absent. In substages C2–C5, the net SO₄²⁻ fluxes had a negative correlation with the NO₃⁻ fluxes: As the NO₃⁻ flux increased from 0.06 to 0.23 e⁻ eq/m²-d, the net SO₄²⁻ flux decreased in parallel, from 0.14 to 0.002 e⁻ eq/m²-d. The total H₂ consumption increased from 0.14 to 0.23 e⁻ eq/m²-d as the NO₃⁻ loading increased, and this was accompanied by a small reduction in the unused-H₂ flux (from 0.014 to 0.006 e⁻ eq/m²-d). These results are consistent with Zhao et al. [38], who reported that SO₄²⁻ removal dropped from 78% to 21% once NO₃⁻ was introduced.

Based on the S mass balance, S⁰ accumulated in the biofilm in substages C2 and C3. (The next section documents the accumulation of S⁰ using XRD.) S⁰ accumulated only when the influent NO₃⁻ concentration was 10 and 20 mg N/L. About 31% of the reduced sulfide was partially oxidized to S⁰ that accumulated in the biofilm when the influent NO₃⁻ concentration was 10 mg N/L (Fig. 4a); this corresponded to 10 mg S/L in the effluent. The accumulated-S⁰ concentrations were 2.7, 0, and 0 mg/L as the influent NO₃⁻ concentration was

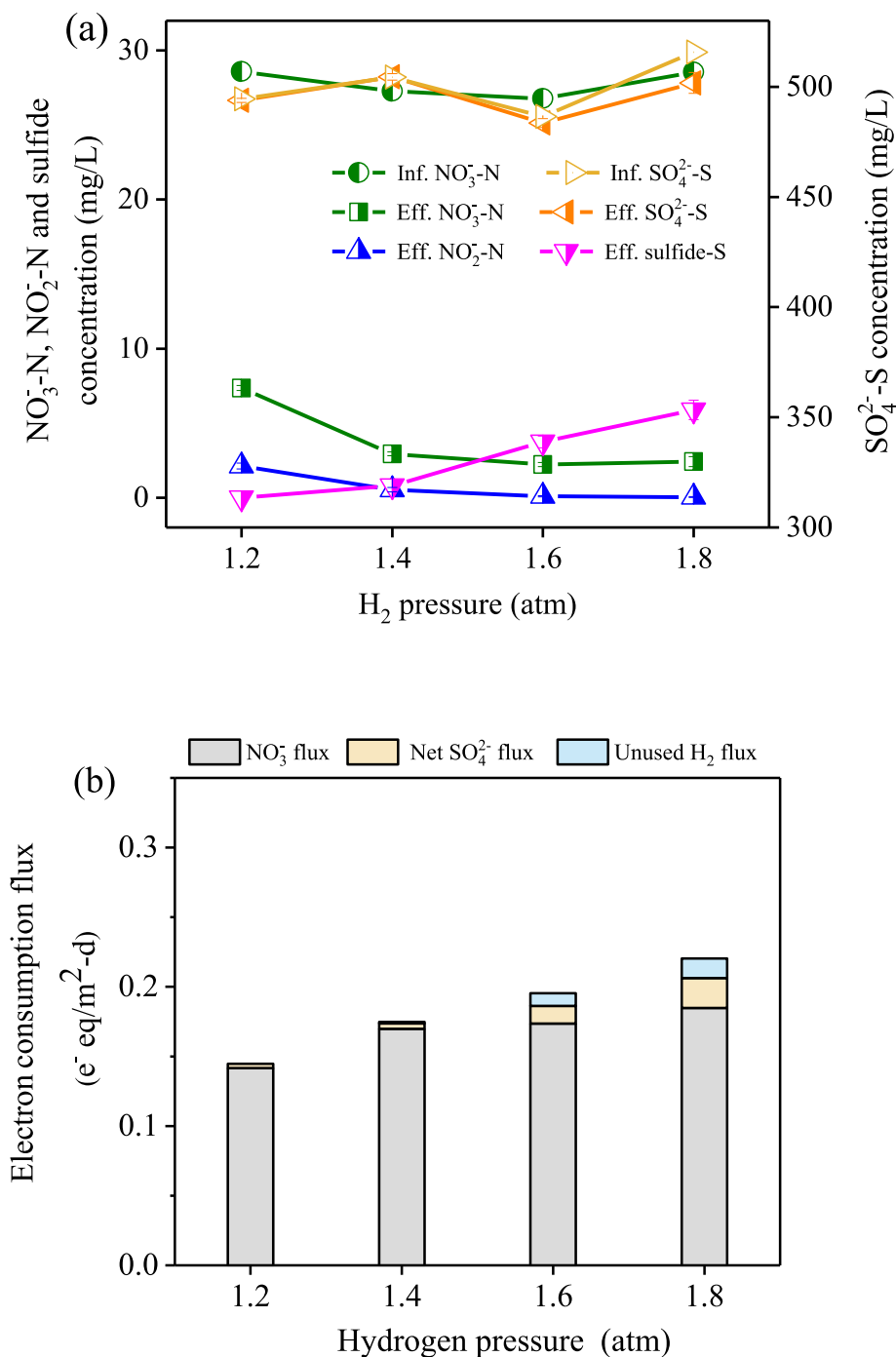


Fig. 3. Results for the B substages, in which the H₂ pressure was increased.

increased to 20, 27, and 38 mg N/L, respectively. The influent S/N mole ratios were 1.4, 0.75, 0.52, and 0.37 for these four NO₃⁻ inputs.

We computed nitrate's electron-equivalent fluxes (shown in Fig. 4b) for oxidation from sulfide to S⁰ (called NO₃⁻ flux 1) and from sulfide to SO₄²⁻ (called NO₃⁻ flux 2) based on the stoichiometry in Eqs. (5) and (6). Sulfide oxidation increased from 0.03 to 0.13 eq/m²-d when the influent NO₃⁻ concentration increased from 0 to 40 mg N/L.

The S/N mole ratio had major control over the accumulation of S⁰, represented as an equivalent S⁰ concentration in the effluent. When nitrate was in short supply as an electron acceptor (i.e., a high S/N ratio), sulfide oxidation stopped at S⁰; however, complete sulfide oxidation was achieved with excess NO₃⁻ due to a low S/N ratio in the influent. The observed use of denitrification for sulfide oxidation with

small S/N ratio is consistent with Liu et al. [23], who used a continuous-flow reactor having sulfide as the electron donor for denitrification. They found that the S⁰ conversion rate increased from 15% to 90% when the influent S/N mole ratio was increased from 0.3 to 1.3.

Re-oxidation was the major reason why net SO₄²⁻ flux was suppressed by NO₃⁻ loading in the C substages, which also accounts for the most sulfide reduction when NO₃⁻ was absent in substage C1. Using NO₃⁻ to oxidize SO₄²⁻ lowered the H₂ demand, because the electrons transferred from H₂ to sulfide flowed to NO₃⁻ when it was the acceptor for sulfide oxidation. While most of the sulfide was fully oxidized back to SO₄²⁻, a modest fraction was retained in the biofilm as S⁰ when the nitrate loading was not too high (substages C2 and C3).

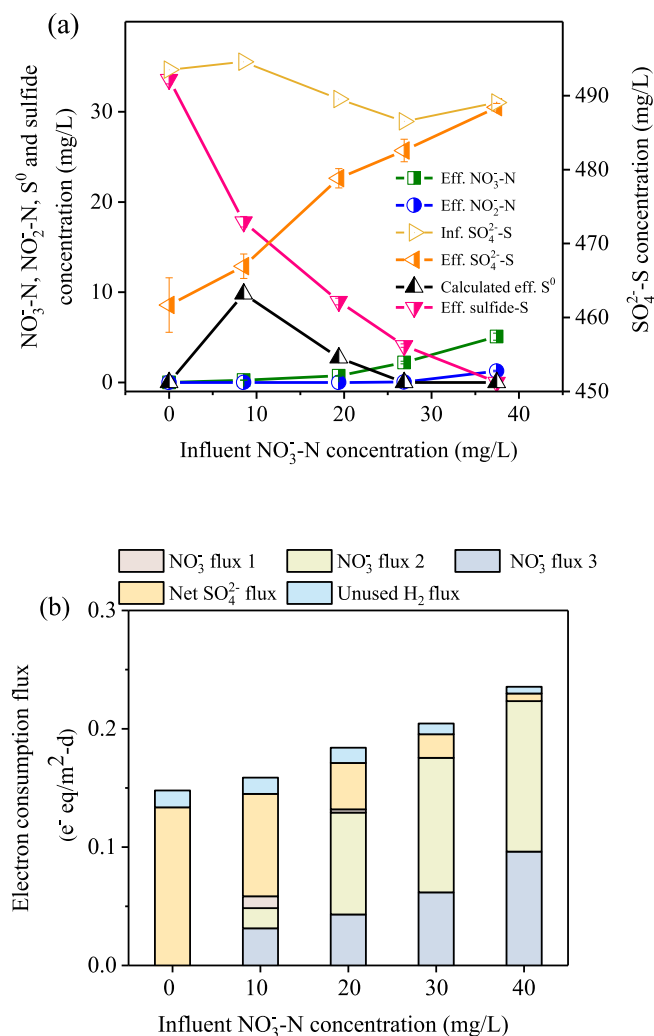


Fig. 4. Results for the C substages, in which the NO_3^- loading was increased.

3.2.4. The accumulation of S^0

In order to document that S^0 precipitated and accumulated in the biofilm during the C substages, we collected biofilm solids from the C substages and analyzed them using XRD. The XRD patterns for biofilm, shown for substage C2 in Fig. 5a, show the diffraction peaks of S^0 at 2θ at 13.2° , 23.5° , and 27.1° (PDF: 13-0141), which prove that S^0 existed in the biofilm. S^0 surface density in biofilms (shown in Fig. 5b) presents the $\mu\text{g S}/\text{cm}^2$ membrane surface area of S^0 for all substages, the results in substage C1, C2, C3, C4, and C5 were 1.6, 34.1, 13.8, 0, and 0, respectively. S^0 accumulated in the biofilm (surface density of the biofilm was $0.55 \text{ mg cell}/\text{cm}^2$) the most in substage C2 and disappeared completely with highest NO_3^- loadings in substages C4 and C5. Substage C3 had about one-third the S^0 concentration of substage C2. This is consistent with the much smaller S^0 accumulation based on mass balance (Fig. 4a), and it may reflect retention of some S^0 accumulated in substage C2. The total loss of S^0 in substages C4 and C5 suggests that they were oxidized as the electron donor for denitrification.

3.3. Regulation of practical wastewater by surface loading control

In stage 4, the MBfR was continually fed with the actual wastewater for 80 days to verify its practicability, the influent concentration of NO_3^- -N and SO_4^{2-} -S were 33 and 470 mg/L, the wastewater-quality properties were shown in Table S4, SI. In Section 3.2, we demonstrated SO_4^{2-} reduction was suppressed by NO_3^- loading that determined by influent concentration. For wastewater that NO_3^- concentration was

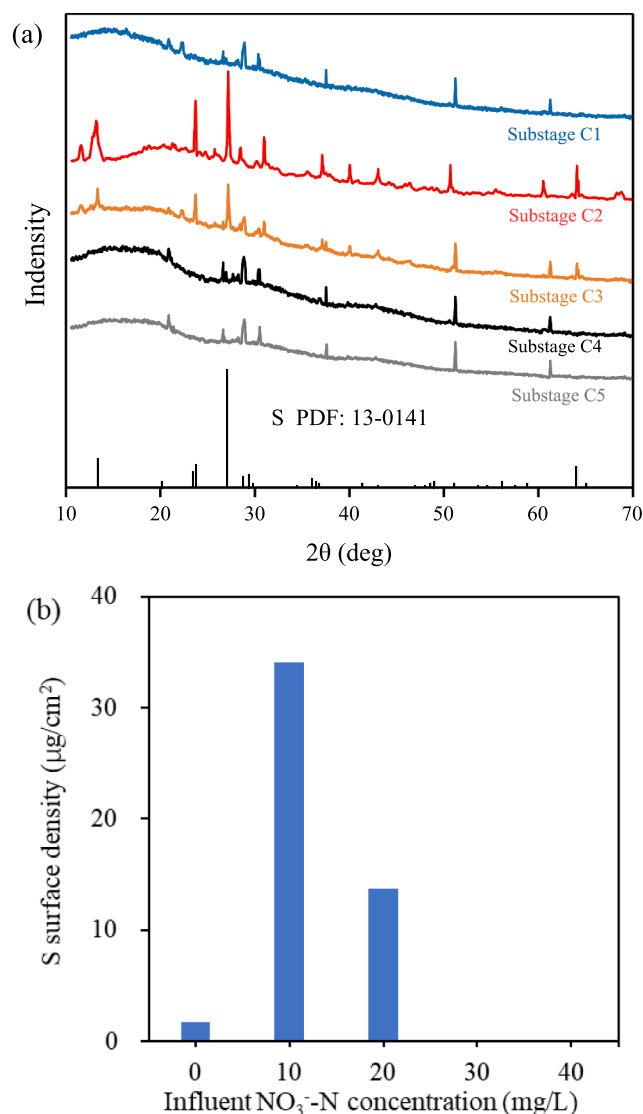


Fig. 5. XRD analysis of biofilms show evidence of S adsorbed on biofilm (a); sulfur surface density in biofilms (b).

certain, we changed the NO_3^- loading by influent flow. To investigate effect of surface loadings of NO_3^- and SO_4^{2-} on their reduction, inflow rate was set as 0.33, 1, and 2 mL/min. The effluent pH was 6.9–7.2, and NO_2^- was not detected. The effluent concentrations of NO_3^- correlated to the increasing influent flow, and their removal fluxes also increased (Fig. 6). The removal flux of NO_3^- ($0.18 \text{ e}^- \text{ eq}/\text{m}^2$ -d, HRT = 10.5 h) was close to that obtained with synthesis water for the same conditions. The onset of SO_4^{2-} reduction occurred at an influent flow of 1 mL/min (HRT of 10.5 h), but longer HRTs resulted in more SO_4^{2-} reduction. Thus, to find an optimal influent flow is a management strategy to achieve NO_3^- reduction but suppress SO_4^{2-} reduction in actual wastewater.

3.4. Microbial community shaped by electron acceptors

We collected samples of the inoculum and the biofilm at the end of stages 1 and 2 for high-throughput sequencing. Fig. 7a summarizes the results at the class level and according to the known abilities to carry out denitrification, sulfate reduction, and sulfide oxidation. As expected, the relative abundance of DB moderately declined in stage 2 (with added SO_4^{2-}) compared with stage 1 (without added SO_4^{2-}), while SRB and SOB increased in stage 2.

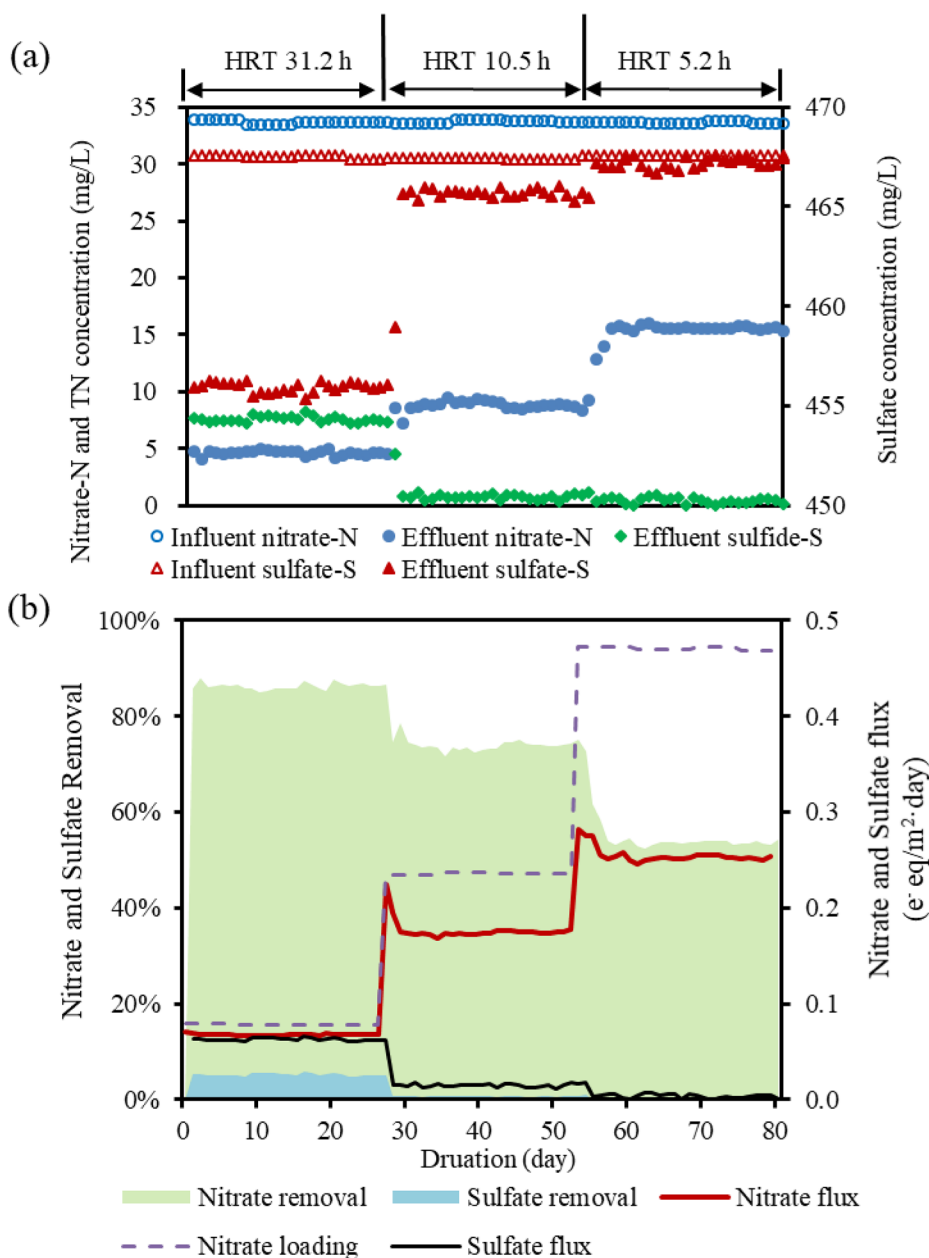


Fig. 6. Performance profiles during stage 4.

3.4.1. Denitrifying groups in the biofilm

Fig. 7b presents the major phylotypes at the genus level. Although phylotypes were diverse in the inoculum, sequences related to the *Betaproteobacteria* class were dominant (44%), and potential denitrifying groups were presented by genera belong to families *Xanthobacteraceae* (6%) and *Xanthomonadaceae* (7%). The relative abundance of DB increased to 65% with complete denitrification in MBfR (stage 1), and the predominant group shifted to the family *Comamonadaceae*, which was dominated by *Hydrogenophaga* (32%), a common denitrifier in MBfRs [7,10]. An important DB in stage 1 was belong to the family *Cyclobacteriaceae* (22%), an alkalophilic denitrifying group that grows in pH of 7–12 [41]. It was apparently enriched in alkaline conditions (pH 8) and disappeared when the effluent pH was below 7 (stage 2).

3.4.2. Absence of net SO_4^{2-} reduction due to sulfur-cycle

Phylotypes related to SO_4^{2-} metabolism were represented by genera *Desulfotomaculum* (5.7%), *Desulfitibacter* (4.3%), and *Dethiobacter* (3.5%). The roles these phylotypes likely played in the

SO_4^{2-} reduction are noteworthy. *Desulfotomaculum*, a known SRB, can use SO_4^{2-} as its electron acceptor [42–44]. In contrast, *Desulfitibacter* utilizes the intermediates SO_3^{2-} or S^0 as electron acceptors, but not SO_4^{2-} [45,46]. *Dethiobacter* uses thiosulfate, polysulfide, and S^0 as electron acceptors [47,48]. Therefore, the presence of *Desulfitibacter* and *Dethiobacter* suggests SO_3^{2-} or S^0 reduction, since they cannot directly metabolize SO_4^{2-} . Additionally, some SRB have metabolic flexibility that helps them persist in a biofilm when SO_4^{2-} is absent [12,38]. *Desulfitibacter* is reported to respire NO_3^- [45], and NO_3^- is normally the preferred electron receptor when SO_4^{2-} and NO_3^- coexist [12,16,33]. Thus, this multi-function genus might act as SRB when it cannot do denitrification, otherwise, it functions as a DB.

SOB belonging to the family *Xanthobacteraceae* were present only after adding SO_4^{2-} (stage 2): The genera *Starkeya* (6.1%) and *Xanthobacter* (12.9%), capable of respiring NO_3^- coupled to sulfide oxidation to SO_4^{2-} or partial oxidation to S^0 , depending on the S/N ratio [49,50].

Occlusive S-cycle in the biofilm driven by SRB and SOB led to less

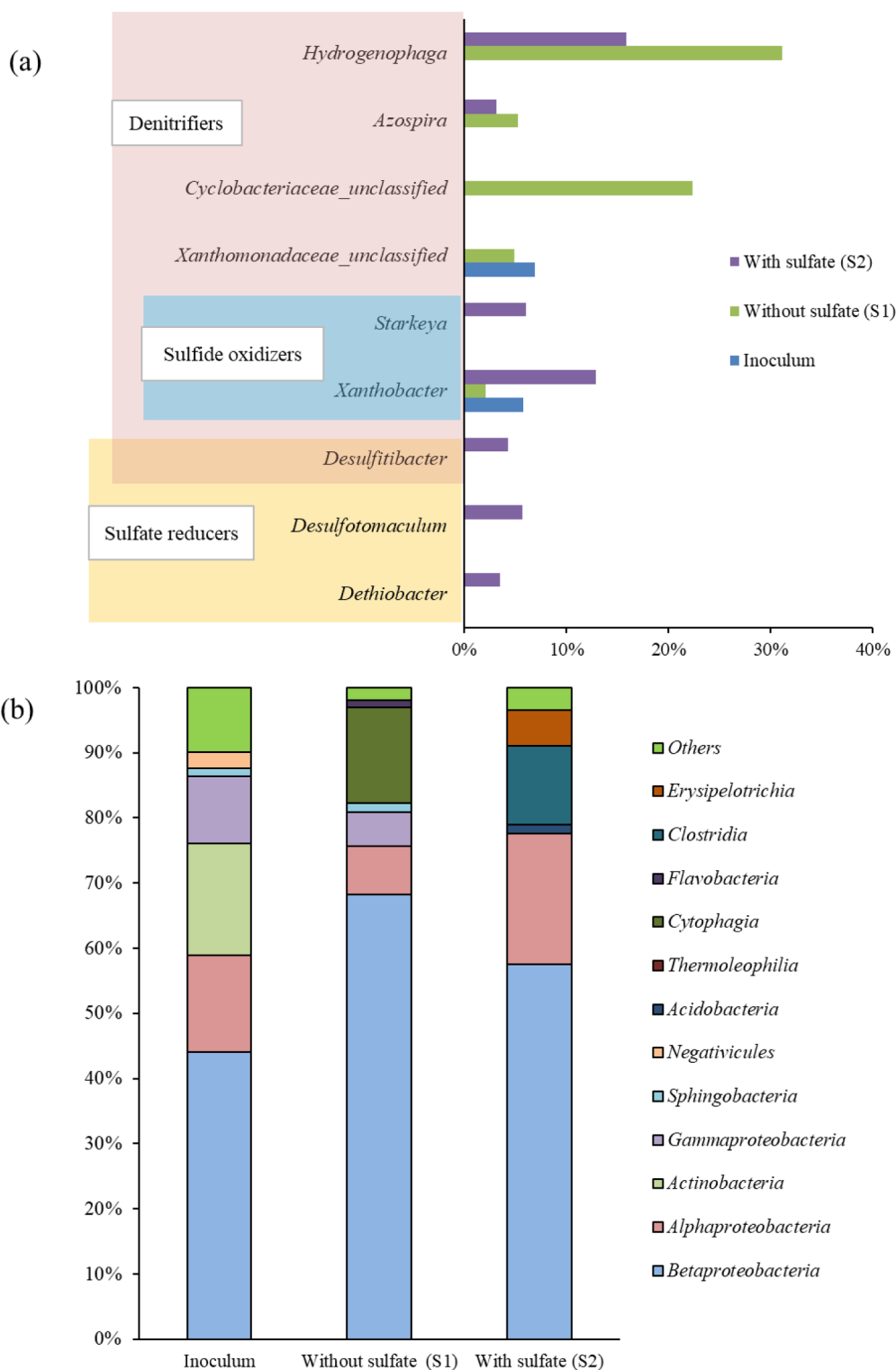


Fig. 7. Phylogenetic profiling of the major microflora in the inoculum and biofilms.

net SO_4^{2-} reduction (shown in Fig. 8). SRB consumed H_2 to reduce SO_4^{2-} to sulfide, whereas SOB continued to oxidize sulfide partially back to SO_4^{2-} couple with NO_3^- reduction. As a result, electron flowed through the sulfide and eventually flowed to the NO_3^- . This S-cycle process might account for the results of Section 3.2.3, an increase of NO_3^- flux decreased net SO_4^{2-} flux through more sulfide oxidation to S^0 or SO_4^{2-} , which also account for the inverse relationship between SO_4^{2-} and NO_3^- reduction fluxes.

4. Conclusions

An MBfR equipped with H_2 and CO_2 membranes was used to study denitrification in high-sulfate containing water. The MBfR gave stable denitrification when using CO_2 as the sole carbon source and pH moderator. While a high SO_4^{2-} loading had negligible effect on NO_3^- reduction, high enough NO_3^- reduction fluxes strongly suppressed SO_4^{2-} reduction. Illumina sequencing, XRD results, and electron-

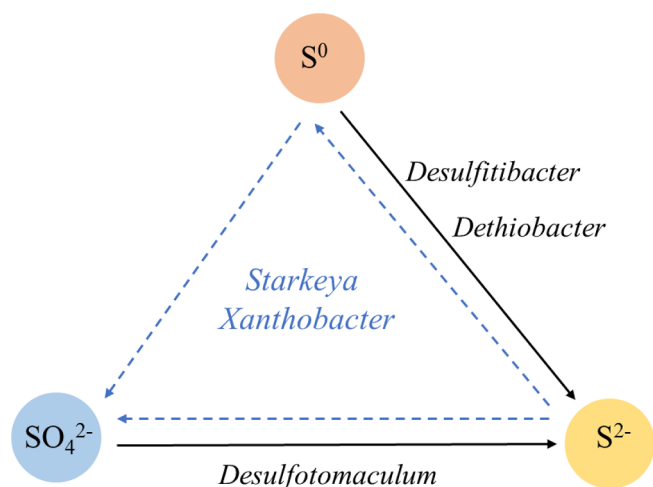


Fig. 8. Functional bacteria of S-cycle in this study.

equivalent mass balances support that SO_4^{2-} reduction was suppressed by increasing NO_3^- loading due to three reasons: SRB abundance was restricted by space competition with DB, some SRB preferred to denitrify, and importantly, SOB oxidized sulfide back to SO_4^{2-} using NO_3^- as the electron acceptor. Therefore, occlusive S-cycle in the biofilm driven by these genera decreases net SO_4^{2-} reduction when SO_4^{2-} and NO_3^- coexist.

Declaration of Competing Interest

The authors declare that they have no known competing financial interests or personal relationships that could have appeared to influence the work reported in this paper.

Acknowledgements

This work is supported by National Natural Science Foundation of China (51678422) and the Fundamental Research Funds for the Central Universities (22120190017).

Appendix A. Supplementary data

Supplementary data to this article can be found online at <https://doi.org/10.1016/j.cej.2019.123831>.

References

- [1] U.S. EPA, 2004 Edition of the Drinking Water Standards and Health Advisories, 2004.
- [2] H.I. Shuval, N. Gruener, Infant methemoglobinemia and other health effects of nitrates in drinking water, *Proc. Conf. Nitrogen Water Pollut.* (2013) 183–193.
- [3] Y. Tang, Z. Zhang, B. Rittmann, H.-S. Lee, Kinetics of anaerobic methane oxidation coupled to denitrification in the membrane biofilm reactor, *Biotechnol. Bioeng.* (2019).
- [4] C. Zhou, A. Ontiveros-Valencia, R. Nerenberg, Y. Tang, B.E. Rittmann, Hydrogenotrophic microbial reduction of oxyanions with the membrane biofilm reactor, *Front. Microbiol.* 9 (2019) 1–14.
- [5] B.E. Rittmann, P.L. McCarty, *Environmental Biotechnology: Principles and Applications*, McGraw-Hill Companies Inc, New York, 2001.
- [6] A. Ontiveros-Valencia, C. Zhou, H.P. Zhao, R. Krajmalnik-Brown, Y. Tang, B.E. Rittmann, Managing microbial communities in membrane biofilm reactors, *Appl. Microbiol. Biotechnol.* 102 (2018) 9003–9014.
- [7] M. Long, Z.E. Ilhan, S. Xia, C. Zhou, B.E. Rittmann, Complete dechlorination and mineralization of pentachlorophenol (PCP) in a hydrogen-based membrane biofilm reactor (MBfR), *Water Res.* 144 (2018) 134–144.
- [8] H.-P. Zhao, A. Ontiveros-Valencia, Y. Tang, B.O. Kim, Z.E. Ilhan, R. Krajmalnik-Brown, B. Rittmann, Using a Two-Stage Hydrogen-Based Membrane Biofilm Reactor (MBfR) to Achieve Complete Perchlorate Reduction in the Presence of Nitrate and Sulfate, *Environ. Sci. Technol.* 47 (2013) 1565–1572.
- [9] C. Zhou, A. Ontiveros-Valencia, Z. Wang, J. Maldonado, H.P. Zhao, R. Krajmalnik-Brown, B.E. Rittmann, Palladium Recovery in a H₂-Based Membrane Biofilm

- Reactor: Formation of Pd(0) Nanoparticles through Enzymatic and Autocatalytic Reductions, *Environ. Sci. Technol.* 50 (2016) 2546.
- [10] C.-Y. Lai, X. Yang, Y. Tang, B.E. Rittmann, H.-P. Zhao, Nitrate Shaped the Selenate-Reducing Microbial Community in a Hydrogen-Based Biofilm Reactor, *Environ. Sci. Technol.* 48 (2014) 3395–3402.
- [11] J. Shapleigh, *The Denitrifying Prokaryotes*, Springer, New York, 2006.
- [12] A. Ontiveros-Valencia, M. Ziv-El, H.P. Zhao, L. Feng, B.E. Rittmann, R. Krajmalnik-Brown, Interactions between Nitrate-Reducing and Sulfate-Reducing Bacteria Coexisting in a Hydrogen-Fed Biofilm, *Environ. Sci. Technol.* 46 (2012) 11289–11298.
- [13] X. Zheng, C. Zhou, Z. Liu, M. Long, Y.-H. Luo, T. Chen, A. Ontiveros-Valencia, B.E. Rittmann, Anaerobic biodegradation of catechol by sediment microorganisms: Interactive roles of N reduction and S cycling, *J. Cleaner Prod.* 230 (2019) 80–89.
- [14] T. Dalsgaard, F. Bak, Nitrate Reduction in a Sulfate-Reducing Bacterium, *Desulfovibrio desulfuricans*, Isolated from Rice Paddy Soil: Sulfide Inhibition, Kinetics, and Regulation, *Appl. Environ. Microbiol.* 60 (1994) 291–297.
- [15] Y. Tang, M. Ziv-El, C. Zhou, J.H. Shin, H.A. Chang, K. Meyer, D. Candelaria, D. Friese, R. Overstreet, R. Scott, Bioreduction of nitrate in groundwater using a pilot-scale hydrogen-based membrane biofilm reactor, *Front. Environ. Sci. Eng. China* 4 (2010) 280–285.
- [16] A. Ontiveros-Valencia, Y. Tang, R. Krajmalnik-Brown, B.E. Rittmann, Managing the interactions between sulfate- and perchlorate-reducing bacteria when using hydrogen-fed biofilms to treat a groundwater with a high perchlorate concentration ☆, *Water Res.* 55 (2014) 215–224.
- [17] K. Saritpongteeraka, S. Chaiprapat, Effects of pH adjustment by parawood ash and effluent recycle ratio on the performance of anaerobic baffled reactors treating high sulfate wastewater, *Bioresour. Technol.* 99 (2008) 8987–8994.
- [18] X. Li, J. Liu, F. Yao, W. Wu, S. Yang, S.M. Mbadinga, J. Gu, B. Mu, Dominance of *Desulfotomaculum* in sulfate-reducing community in high sulfate production-water of high temperature and corrosive petroleum reservoirs, *Int. Biodeterior. Biodegrad.* 114 (2016) 45–56.
- [19] A.H. Kalkonen, J.A. Puhakka, Sulfate reduction based bioprocesses for the treatment of acid mine drainage and the recovery of metals, *Eng. Life Sci.* 7 (2007) 541–564.
- [20] R.K. Srivastava, W. Jozewicz, Flue gas desulfurization: the state of the art, *J. Air Waste Manag. Assoc.* 51 (2001) 1676–1688.
- [21] E. Vaiopoulou, P. Melidis, A. Aivasidis, Sulfide removal in wastewater from petrochemical industries by autotrophic denitrification, *Water Res.* 39 (2005) 4101–4109.
- [22] H. Guo, C. Chen, D.-J. Lee, A. Wang, N. Ren, Sulfur–nitrogen–carbon removal of *Pseudomonas* sp. C27 under sulfide stress, *Enzyme Microb. Technol.* 53 (2013) 6–12.
- [23] C. Liu, W. Li, X. Li, D. Zhao, B. Ma, Y. Wang, F. Liu, D.-J. Lee, Nitrite accumulation in continuous-flow partial autotrophic denitrification reactor using sulfide as electron donor, *Bioresour. Technol.* 243 (2017) 1237–1240.
- [24] S. An, K. Tang, M. Nemat, Simultaneous biodesulfurization and denitrification using an oil reservoir microbial culture: Effects of sulphide loading rate and sulphide to nitrate loading ratio, *Water Res.* 44 (2010) 1531–1541.
- [25] K.C. Lee, B.E. Rittmann, Applying a novel autohydrogenotrophic hollow-fiber membrane biofilm reactor for denitrification of drinking water, *Water Res.* 36 (2002) 2040–2052.
- [26] Y. Tang, C. Zhou, M. Ziv-El, B.E. Rittmann, A pH-control model for heterotrophic and hydrogen-based autotrophic denitrification, *Water Res.* 45 (2011) 232–240.
- [27] H. Jong Hyuk, C. Nazim, J.A. Oleszkiewicz, Inorganic precipitation during autotrophic denitrification under various operating conditions, *Environ. Technol.* 30 (2009) 1475–1485.
- [28] M.C. Ziv-El, B.E. Rittmann, Systematic evaluation of nitrate and perchlorate bioreduction kinetics in groundwater using a hydrogen-based membrane biofilm reactor, *Water Res.* 43 (2009) 173–181.
- [29] H.W. Kim, J. Cheng, B.E. Rittmann, Direct membrane-carbonation photobioreactor producing photoautotrophic biomass via carbon dioxide transfer and nutrient removal, *Bioresour. Technol.* 204 (2016) 32–37.
- [30] S. Xia, X. Xu, C. Zhou, C. Wang, L. Zhou, B.E. Rittmann, Direct delivery of CO₂ into a hydrogen-based membrane biofilm reactor and model development, *Chem. Eng. J.* 290 (2016) 154–160.
- [31] S. Xia, C. Wang, X. Xu, Y. Tang, Z. Wang, Z. Gu, Y. Zhou, Bioreduction of nitrate in a hydrogen-based membrane biofilm reactor using CO₂ for pH control and as carbon source, *Chem. Eng. J.* 276 (2015) 59–64.
- [32] H.W. Kim, A.K. Marcus, J.H. Shin, B.E. Rittmann, Advanced Control for Photoautotrophic Growth and CO₂-Utilization Efficiency Using a Membrane Carbonation Photobioreactor (MCPBR), *Environ. Sci. Technol.* 45 (2011) 5032–5038.
- [33] J. Chung, Nerenberg Robert, Bruce E. Rittmann, Bioreduction of selenate using a hydrogen-based membrane biofilm reactor, *Environ. Sci. Technol.* 40 (2006) 1664–1671.
- [34] J.D. Cline, Spectrophotometric Determination of Hydrogen Sulfide in Natural Waters, *Limnol. Oceanogr.* 14 (1969) 454–458.
- [35] S. Xia, Y.H. Zhang, F.H. Zhong, A continuous stirred hydrogen-based polyvinyl chloride membrane biofilm reactor for the treatment of nitrate contaminated drinking water, *Bioresour. Technol.* 100 (2009) 6223–6228.
- [36] Y. Tang, C. Zhou, S.W.V. Ginkel, A. Ontiveros-Valencia, J. Shin, B.E. Rittmann, Hydrogen permeability of the hollow fibers used in H₂-based membrane biofilm reactors, *J. Membr. Sci.* 407–408 (2012) 176–183.
- [37] J.G. Caporaso, J. Kuczynski, J. Stombaugh, K. Bittinger, F.D. Bushman, E.K. Costello, N. Fierer, A.G. Peña, J.K. Goodrich, J.I. Gordon, G.A. Huttley, S.T. Kelley, D. Knights, J.E. Koenig, R.E. Ley, C.A. Lozupone, D. McDonald,

- B.D. Muegge, M. Pirrung, J. Reeder, J.R. Sevinsky, P.J. Turnbaugh, W.A. Walters, J. Widmann, T. Yatsunenko, J. Zaneveld, R. Knight, QIIME allows analysis of high-throughput community sequencing data, *Nat. Methods* 7 (2010) 335.
- [38] H.P. Zhao, Z.E. Ilhan, A. Ontiveros-Valencia, Y.N. Tang, B.E. Rittmann, R. Krajmalnik-Brown, Effects of multiple electron acceptors on microbial interactions in a hydrogen-based biofilm, *Environ. Sci. Technol.* 47 (2013) 7396–7403.
- [39] D.R. Noguera, G.A. Brusseau, B.E. Rittmann, D.A. Stahl, Unified model describing the role of hydrogen in the growth of *Desulfovibrio vulgaris* under different environmental conditions, *Biotechnol. Bioeng.* 59 (1998) 732–746.
- [40] Y. Tang, A. Ontiveros-Valencia, L. Feng, C. Zhou, R. Krajmalnik Brown, B.E. Rittmann, A biofilm model to understand the onset of sulfate reduction in denitrifying membrane biofilm reactors, *Biotechnol. Bioeng.* 110 (2013) 763–772.
- [41] T.N.R. Srinivas, S. Aditya, V. Bhumika, P.A. Kumar, *Lunatimonas lonarensis* gen. nov., sp. nov., a haloalkaline bacterium of the family Cyclobacteriaceae with nitrate reducing activity, *Syst. Appl. Microbiol.* 37 (2014) 10–16.
- [42] So-Jeong Kim, Hee-Ji Hong, Sung-Keun Rhee, In-Tae Cha, Hae-Won Lee, *Desulfotomaculum tongense* sp. nov., a moderately thermophilic sulfate-reducing bacterium isolated from a hydrothermal vent sediment collected from the Tofua Arc in the Tonga Trench, *Antonie Van Leeuwenhoek* 104 (2013) 1185–1192.
- [43] J. Pilar, J. Thomas, P. Sheila, D.R. Sims, J.C. Detter, L. Athanasios, C.S. Han, N.S. Wigginton, G. Terry, B.L. Rizlan, The genome of the Gram-positive metal- and sulfate-reducing bacterium *Desulfotomaculum reducens* strain MI-1, *Environ. Microbiol.* 12 (2010) 2738–2754.
- [44] S. Spring, A. Lapidus, M. Schröder, D. Gleim, D. Sims, L. Meincke, T. Glavina Del Rio, H. Tice, A. Copeland, J.-F. Cheng, S. Lucas, F. Chen, M. Nolan, D. Bruce, L. Goodwin, S. Pitluck, N. Ivanova, K. Mavromatis, N. Mikhailova, A. Pati, A. Chen, K. Palaniappan, M. Land, L. Hauser, Y.-J. Chang, C.D. Jeffries, P. Chain, E. Saunders, T. Brettin, J.C. Detter, M. Göker, J. Bristow, J.A. Eisen, V. Markowitz, P. Hugenholtz, N.C. Kyrpides, H.-P. Klenk, C. Han, Complete genome sequence of *Desulfotomaculum acetoxidans* type strain (5575), *Standards Genomic Sci.* 1 (2009) 242.
- [45] M.B. Nielsen, K.U. Kjeldsen, K. Ingvorsen, *Desulfitibacter alkalitolerans* gen. nov., sp. nov., an anaerobic, alkalitolerant, sulfite-reducing bacterium isolated from a district heating plant, *Int. J. Syst. Evol. Microbiol.* 56 (2006) 2831–2836.
- [46] D.Y. Sorokin, G. Muyzer, Haloalkaliphilic spore-forming sulfidogens from soda lake sediments and description of *Desulfitispora alkaliphila* gen. nov., sp. nov., *Extremophiles* 14 (2010) 313–320.
- [47] E.D. Melton, D.Y. Sorokin, L. Overmars, A.L. Lapidus, M. Pillay, N. Ivanova, T.G. del Rio, N.C. Kyrpides, T. Woyke, G. Muyzer, Draft genome sequence of *Dethiobacter alkaliphilus* strain AHT1T, a gram-positive sulfidogenic polyextremophile, *Standards Genomic Sci.* 12 (2017).
- [48] D.Y. Sorokin, T.P. Tourova, M. Musmann, G. Muyzer, *Dethiobacter alkaliphilus* gen. nov. sp. nov., and *Desulfurivibrio alkaliphilus* gen. nov. sp. nov.: two novel representatives of reductive sulfur cycle from soda lakes, *Extremophiles* 12 (3) (2008) 431–439.
- [49] J. De Ley, M. Van Poucke, The formation of sulphite during the oxidation of thio-sulphate by *Thiobacillus novellus*, *Biochim. Biophys. Acta* 50 (1961) 371–373.
- [50] D.P. Kelly, J.K. Shergill, W.P. Lu, A.P. Wood, Oxidative metabolism of inorganic sulfur compounds by bacteria, *Antonie Van Leeuwenhoek* 71 (1997) 95–107.